Integrated microscopy for real-time imaging of mechanotransduction studies in live cells

Andreea Trache
Texas A&M Health Science Center
Cardiovascular Research Institute
College of Medicine
Department of Systems Biology and
 Translational Medicine
College Station, Texas 77843-1114
 and
Texas A&M University
Department of Biomedical Engineering
College Station, Texas 77840
E-mail: trache@tamu.edu

Soon-Mi Lim
Texas A&M Health Science Center
Cardiovascular Research Institute
College of Medicine
Department of Systems Biology and
 Translational Medicine
College Station, Texas 77843-1114

Abstract. Mechanical force is an important stimulus and determinant of many vascular smooth muscle cell functions including contraction, proliferation, migration, and cell attachment. Transmission of force from outside the cell through focal adhesions controls the dynamics of these adhesion sites and initiates intracellular signaling cascades that alter cellular behavior. To understand the mechanism by which living cells sense mechanical forces, and how they respond and adapt to their environment, a critical first step is to develop a new technology to investigate cellular behavior at subcellular level that integrates an atomic force microscope (AFM) with total internal reflection fluorescence (TIRF) and fast-spinning disk (FSD) confocal microscopy, providing high spatial and temporal resolution. AFM uses a nanosensor to measure the cell surface topography and can apply and measure mechanical force with high precision. TIRF microscopy is an optical imaging technique that provides high-contrast images with high z-resolution of fluorescently labeled molecules in the immediate vicinity of the cell–coverslip interface. FSD confocal microscopy allows rapid 3-D imaging throughout the cell in real time. The integrated system is broadly applicable across a wide range of molecular dynamic studies in any adherent live cells, allowing direct optical imaging of cell responses to mechanical stimulation in real time. © *2009 Society of Photo-Optical Instrumentation Engineers.* [DOI: 10.1117/1.3155517]

Keywords: integrated microscopy; atomic force microscopy; spinning-disk confocal; total internal reflection fluorescence.

Paper 08353RR received Oct. 2, 2008; revised manuscript received Apr. 2, 2009; accepted for publication Apr. 4, 2009; published online Jun. 30, 2009.

1 Introduction

As noted in the 1998 National Institutes of Health Bioengineering Consortium Report: "New developments in microscopies are providing crucial information and essential approaches for understanding the structure function of cells and molecules. Molecular and cellular bioengineering is a rapidly evolving multidisciplinary area capitalizing on these technologies to create advances in research in many vital areas." We are presenting here a state of the art technology that offers novel applications in real-time assessment of mechanotransduction dynamics in live cells by combining the structural and functional resolving power of the atomic force microscope (AFM) with rapid optical imaging at high spatial and temporal resolution provided by total internal reflection fluorescence (TIRF) and fast-spinning disk (FSD) confocal imaging. This unique integrated microscopy technology facilitates 4-D real-time biophysical studies directed toward the alteration of the intracellular force balance within cells, along with resulting functional modulations at distant sites (i.e., junctional and focal adhesions). Real-time analysis is essential for direct observations of cellular responses to mechanical or chemical stimuli, and to avoid distortion or loss of cellular components during specimen preparation, which can occur using conventional fixation and antibody-based localization studies.

The present work outlines significant improvement in our previous NanoFluor integrated microscope design[1] that combined AFM with TIRF, interference reflection microscopy, and Forster resonance energy transfer. The improved microscope is particularly well suited to study focal adhesions and cytoskeletal dynamics under AFM mechanical stimulation. By combining the AFM[2] with rapid optical imaging using FSD confocal imaging[3] in a single instrument, substantial progress in real-time monitoring of mechanotransduction dynamics in live cells is possible. The fast-spinning disk confocal is a multibeam scanning method that permits fast scanning at high frame rates as the result of a dual-disk system, pinhole and microlens, that is synchronized with a charge-coupled device (CCD) detector. This tandem arrangement allows for enhanced detection of both low fluorescence signals and real-time image collection. In this way one can rapidly section living cells in 3-D spatial imaging over time to study the cytoskeletal dynamics with minimal exposure of cells to light, preventing cell phototoxicity. In addition, TIRF[4] provides high contrast images that contain high resolution details of cells grown on coverslips with excellent z-resolution

Address all correspondence to: Andreea Trache, Ph.D., 336 Reynolds Medical Bldg., MS 1114, Texas A&M Health Science Center, College Station, TX 77843-1114. Tel: 979-845 7990; Fax: 979-862 4638; E-mail: trache@tamu.edu

($\sim$100 nm depth). Due to minimal exposure of cells to light, TIRF images have very low background fluorescence.

Therefore, by combing these three different techniques, it is now possible to: image cellular processes with high spatial resolution or stimulate the apical cell surface using AFM; perform quantitative time-lapse imaging of the cell-coverslip interface using TIRF; and carry out rapid confocal sectioning in living cells over extended periods of time while studying molecular dynamics and protein translocation between different subcellular structures. Consequently, the integrated microscope described here offers a comprehensive view of mechanotransduction processes from the micrometer to nanometer scale in living cells.

Transmission of force is a classical physical concept applied to live cell dynamics, intracellular protein translocation, and transduction of mechanical signals along intracellular pathways. Multiple dynamic processes trigger changes in cell-cell and cell-matrix adhesions in the vascular wall, resulting in cell growth, motility, contraction, or mechanotransduction. Endothelial and vascular smooth muscle cells reside in a mechanically active environment that changes continuously. Adaptations to these local forces results in realignment of the cytoskeleton and redistribution of the numerous constituents of focal adhesions (FA) and junctional adhesion (JA) sites. The mechanism by which cells sense and respond to mechanical stimuli and the signaling pathways that drive these responses are at a relative early stage of investigation. The current understanding of the molecular processes that induce FA and JA remodeling involving force generation at a scale of pico- to nano-Newtons and a time scale of milliseconds is far from complete. The integrated instrument described here enables quantitative monitoring of rapid molecular changes and provides an important new tool for the study of transduction mechanisms initiated by agonist-induced signaling or external mechanical forces on cells. Generated data will provide new knowledge relating changes in intracellular force balance to the molecular mechanisms by which cytoskeleton communicates a chemical or mechanical stimulus to distant sites. The applications presented here employing microscopy technology that integrates optical and nonoptical scanning techniques are focused on the study of vascular cells. However, the instrument has broad applications to analysis of cellular physiology across a wide variety of adherent cell types.

The cytoskeleton and focal adhesions are dynamic structures that assemble, disperse, and turn over as cells migrate or respond to mechanical forces. They have significant roles in regulating the contractile function, cell growth, survival, and gene expression. Knowledge of the specific distribution and activity of protein constituents and their molecular dynamics will enhance our understanding of how cells detect and respond to structural and functional properties of the extracellular matrix and to neighboring cells.

The cytoskeletal network confers tensile strength to the cell. Actin, the primary cytoskeletal structural protein, together with microtubules determine cell shape. Cell shape stability depends on a network of self-equilibrating structural components, some of which are in tension and others that are in compression.[5] Thus, in cultured vascular smooth muscle cells (VSMC) and endothelial cells, as in any other anchorage-dependent cells, external mechanical stresses are imposed on a preexisting force equilibrium generated by cytoskeletal tension.[6–12] Forces are transmitted as solid mechanical stresses that are distributed throughout the cell via the cytoskeleton. Intracellular stresses may then be transmitted to neighboring cells via JA, and to the underlying matrix via FA at the basal cell surface.

Focal adhesions are critical points for the regulation of actin organization as well as the bidirectional transfer of mechanochemical perturbation[13–20] between the extracellular matrix (ECM) and cytoskeleton. They contain clusters of integrins (transmembrane proteins) that physically link the ECM to the cytoskeleton via a number of specific proteins, including talin, focal adhesion kinase, vinculin, α-actinin, and paxillin. During cellular contraction, specific proteins undergo orientation changes, become phosphorylated,[21–23] or translocate away from the FA (e.g., zyxin[24–26]). Which proteins are absolutely required for the formation of FA is still under investigation, and the order in which these proteins bind integrins to actin or to each other is only partially understood.[18,19]

At the present time it is unclear how a change in the intracellular force balance induces molecular mechanisms by which the cytoskeleton influences FA and JA reorganization and how FA and JA proteins cooperate to respond to mechanical force.

2 Imaging across Biological Spatial and Temporal Scales

"*Many of the most important mechanistic questions in cell biology might be rapidly answered if only we had molecular video electron microscopes—that is, the ability to nondestructively image specific molecules with the resolution of electron microscopy in real time.*"[27]

Important signaling events at cellular level take place in a domain smaller than 500 nm. In epifluorescence microscopy, the diffraction limits the resolution to about 250 nm in the xy plane and is even lower along the z axis. As mentioned before, each imaging technique has its own spatial and temporal limitations. Combinations of optical imaging techniques with atomic force microscopy may overcome some of these spatial and temporal challenges.[28–30] Advantages of FSD confocal and TIRF imaging techniques combined with AFM are discussed next.

Fast-spinning disk confocal is a multibeam scanning method that allows rapid scanning of samples at high frame rates,[3,31–33] being particularly well suited to live cell imaging due to the lower levels of photobleaching and phototoxicity capabilities of this technology. This instrument involves a fully motorized Yokogawa scanning head with a dual-disk system, pinhole and microlens disks, which are perfectly aligned. The size of the pinholes is fixed, being optimal for a specific objective (100×1.4 NA), and will be suboptimal for z-sectioning with a different objective. In this type of confocal microscope, the NA and the objective lens magnification are important, because the zoom-in option is not available. When compared with a classical laser scanning confocal microscope, z-resolution is limited, being dictated primarily by the spacing of the pinholes on the disk. The tandem pinhole-microlens disk partially compensate for this by directing more light through the pinholes, with the same rejection of the out-of-focus light by the disk. The actual image capture speed of this confocal system is limited only by the CCD camera used,

Table 1 Comparison of FSD confocal and TIRF microscopy. For both imaging methods, the acquisition speed is limited only by CCD camera speed and photon collection efficiency (e.g., signal-to-noise ratio).

FSD confocal	TIRF
Optically scanning the entire cell body	Wide-field illumination only at the cell-coverslip interface
Out-of-focus fluorescence rejected by the pinhole disk	No out-of-focus fluorescence, low background
Illuminates the entire cell, risk of photobeaching	Illuminates only the basal cell area (plane of interest), reduced photobleaching

and is discussed further in the CCD camera section.

TIRF microscopy represents a method of exciting and visualizing fluorophores present in the near-membrane region of live cells grown on glass coverslips.[4,34–39] Any movement of fluorescent-tagged proteins within FA or in the immediate proximity of the cell membrane can be monitored in real time. This type of excitation can be used to obtain high contrast fluorescence images, with very low background and virtually no out-of-focus light. The confinement of fluorescence excitation to the near-field interface produces minimal exposure of cells to light in any other planes within the sample. While resolution in optical microscopy is usually diffraction limited by the wavelength of light, this optical imaging technique allows imaging of cellular structures at the coverslip-cell interface with a higher z-resolution (i.e., <100 nm) than confocal microscopy (~ 300 nm) in a wide-field approach. Table 1 presents the main differences between TIRF and confocal imaging.

AFM[2] is an attractive tool for biological applications such as live cell imaging and single molecule force spectroscopy,[40–45] by providing structural, mechanical and functional information at nanometer resolution under physiological conditions. The principle of operation of the AFM is very similar to that of a stylus profilometer—a sharp cantilever tip interacts with the sample surface sensing the local forces between the molecules at the tip and at the sample surface. Due to the fact that no light is involved in acquiring the sample properties, the resolution achieved by the AFM is limited only by the tip radius and the spring constant of the cantilever. When used for imaging live cells, AFM is relatively slow compared with optical imaging (minutes/image). However, when used as a force measurement tool or mechanical stimulation tool, the simultaneous use of AFM with optical imaging enables functional assessment of dynamic processes within live cells.

3 Challenges of Integrating Fast-Spinning Disk Confocal and Total Internal Reflection Fluorescence Microscopy with Atomic Force Microscopy

Specific challenging design requirements are involved in the instrument integration process, requiring customized mechanical and optical components. Integration of the optical systems with the AFM is possible by mounting the AFM scanner on an inverted microscope platform Olympus IX-81. The system layout is presented in Fig. 1. The key element for

preserving all features of a fluorescence microscope is a customized AFM stage[1] that replaces the regular microscope stage, and an open AFM scan head design (Bioscope SZ Hybrid Scanner, Veeco Instruments, Santa Barbara, California). This type of stage is not available in any commercial AFM at this time. As configured, our microscope system allows full turret rotation, full access to the objective lens correction collars, and oil/water loading at the objective lens without moving the sample that is fixed by a magnetic holder.

Special attention was paid toward insulating the integrated microscope from building and acoustic vibrations that can affect or even destroy the AFM measurements. The integrated
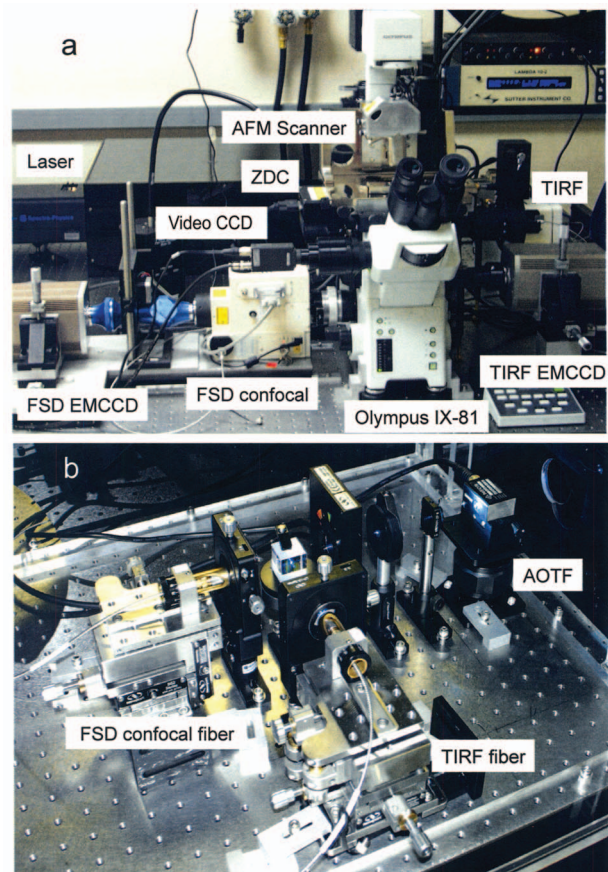

Fig. 1 (a) Layout of the integrated microscope. (b) Layout of the laser-to-fiber optical train (see Fig. 2).
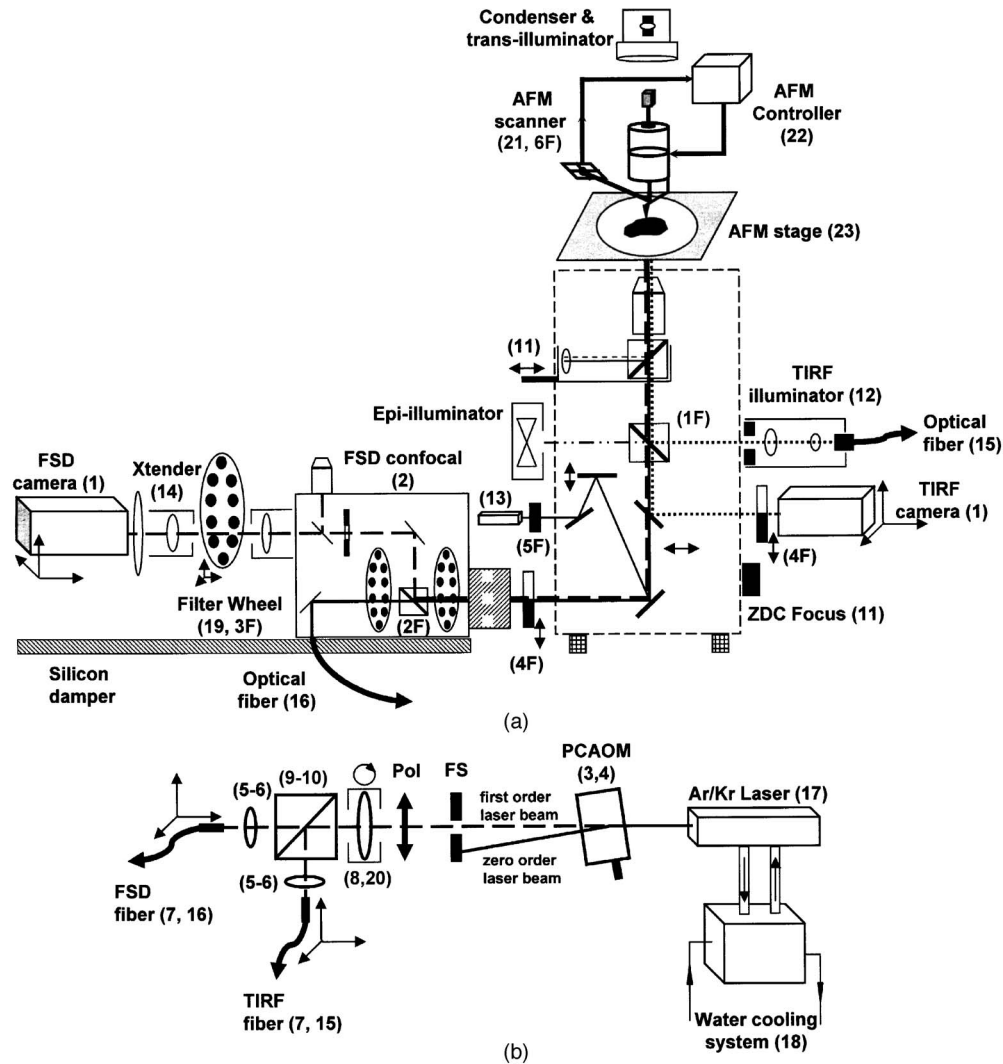
Fig. 2 (a) Diagram of the integrated microscope layout. The entire optical train on the FSD confocal sits on a silicon damper pad that isolates the Yokogawa unit from the optical table. Further vibration isolation is achieved by decoupling the flange between the microscope and FSD confocal, so that no direct mechanical connection exists between the two components. The microscope itself sits on adjustable legs (along the z axis). The optical alignment is performed such that the primary FSD confocal camera is in register with the microscope focal plane in an open beam coupling configuration. The ZDC module is placed between the turret and the microscope objective. On the right-hand side, we placed the TIRF illuminator and its CCD camera. (b) Diagram of the laser-to-fiber optical train. FS is field stop, and POL-polarizer. The optical filters are listed in Table 2 and the main components are listed in Table 3.

microscope and the laser head are placed on a research-grade vibration-insulation tabletop (Newport, Irvine, California). A detailed presentation of vibration isolation, cooling, and electrical wiring requirements were presented elsewhere.[1] While camera cooling fans and other drivers containing fans and moving parts were isolated from the main vibration-isolation table by placing them on a self-standing shelf, this is not possible for the Yokogawa scanner head. The scanner that rotates at 5000 rot/min must be placed in the immediate vicinity of the microscope, having its optical path aligned with the microscope optical path. This important source of vibration was eliminated by designing an open-coupling flange between the scanner head and the microscope, and by placing the scanner on a silicon damper pad that isolates the scanner from the tabletop [Fig. 2(a)].

The optical lever principle used in the AFM scanner to detect the cantilever deflection consists of a laser beam coming from a laser diode in the scanning head that is reflected off the back of the cantilever onto a photodetector. The laser diode emits at 693 nm and was chosen far from the spectral range of wavelengths used for fluorescence measurements. It is known that laser diodes have a broad emission spectrum. To optimize the spectrum output and minimize its interference with the fluorescence, a notch optical filter was mounted into the AFM scanner (Fig. 3). Moreover, even filtered in this way, light coming from the laser diode reaches both cameras, quenching the dim fluorescence, and also reaches the oculars, making impossible the use of microscope eyepieces while the AFM is turned on. Thus, a different filter was designed to block the light of the laser diode and was placed in front of
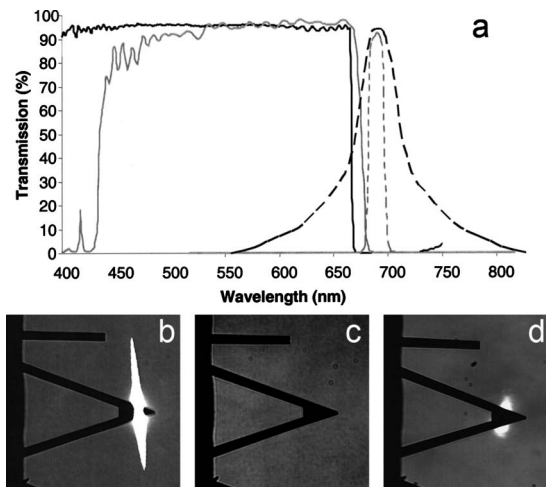
Fig. 3 (a) Transmission curves for the optical filters necessary to exclude the AFM laser diode from the fluorescence path: solid black line—ET670sp is placed in front of the EMCCD and eye pieces; gray line—ET680sp is placed in front of the video camera; dotted line—notch filter in the AFM head; dashed line—generic spectra of a laser diode emitting at 690 nm. The laser diode spectrum is wide enough to bleed through into the visible spectrum suppressing the fluorescence signal. (b) The AFM laser diode light captured by the EMCCD without the notch filter in place (to be able to capture an image that does not completely blank the EMCCD, an extra 647-nm filter was set in the optical path). (c) When the notch filter is mounted in the AFM head, the laser diode light is suppressed. Both images in (b) and (c) were captured with the protection filter in place (solid black line in (a)). (d) The laser diode light is visible to the video camera for an easy alignment of the optical lever [video filter in place is the gray line in (a)].

both cameras and oculars. A limitation introduced by this filter results in blocking the visible spectrum in the red wavelengths (>670 nm), such that dyes like CY5 cannot be used in simultaneous measurements with AFM. This limitation is easily overcome when AFM is not in use, by placing these blocking filters in specially designed sliders that allow sliding the blocking filter in and out of the optical path for TIRF and FSD confocal. For alignment purposes of the AFM optical lever, it is useful to see some of the laser diode light on the video camera used for the optical lever alignment. This required the design of a different optical filter that partially blocks the diode beam in front of the video camera, such that only a small spot of light is visible in the field of view, allowing for a precise alignment of the optical lever.

A user-friendly design of the filter combinations necessary for different applications with the spinning disk confocal required an external filter wheel (Sutter Instruments, Novato, California) to be mounted at the out-put path of the scanning unit. Therefore, different combinations of two or three channels for confocal imaging are possible without moving the filters in the optical path while scanning. All optical filters were provided by Chroma Technologies (Brattleboro, Vermont) and are included in Table 2. The extension of the optical path to the camera was possible by using an optical extender from Optical Insights (Tucson, Arizona) that ensured a good focused image projected on the camera chip without introducing optical aberrations.

A z-drift compensator (ZDC) mounted between the turret and objective nosepiece [Fig. 2(a)] allows for locating the

specimen-coverslip interface with high precision. The ZDC module uses a 785-nm laser diode to find with high precision the upper surface of the coverslip. The ZDC autofocus routine is faster than a conventional microscope autofocus, and is not affected by changes in contrast or fluorescence intensity in the filed of view. Thus, ZDC represents an important addition, providing an optimal solution for long-term time-lapse TIRF experiments where maintenance of the focal plane is critical. Note that TIRF laser alignment is affected by the ZDC module. If the ZDC is to be employed, the laser alignment must be performed with the ZDC module in the optical path. The ZDC autofocus is also used in time-lapse confocal imaging.

4 Description of the Integrated Microscope System

The overall schematic of the integrated microscope shown in Fig. 1 is presented in Fig. 2, and a detailed list of components is presented in Tables 2 and 3. Additional information regarding laser illumination and image acquisition systems are presented next.

4.1 Laser Illumination System and Optical Fiber Alignment

The integrated microscope requires two different illumination ports, one for TIRF and the other for FSD confocal. Thus, a Stabilite 2018-RM 2.5 W Ar-Kr white laser (Spectra Physics, Mountain View, California) is used to feed both illuminators by single-mode optical fibers (Oz Optics, Canada). The laser is run in white mode and is coupled with the microscope, as presented in Fig. 2(b). The polychromatic acusto-optic modulator (PCAOM) provides a controlled first-order output beam. It allows fine tuning of the laser wavelength by changing the rf frequency, and controls the laser line power by changing the rf power applied to the crystal. The crystal mount allows fine z-axis movement and optimal selection of the Bragg angle of the PCAOM to achieve the highest beam power for the first-order beam. An eight-channel Neos driver controls the PCAOM with 10-μsec switching time between laser lines. For stability during experiments, the laser is operated in constant power mode, with the laser aperture set to aperture 5 as an optimal value to ensure good mode structure and output power for each wavelength.

The PCAOM is followed by an iris aperture and a clean-up polarizer. The achromat half-wave plate (Thorlabs, Newton, New Jersey) and the cube beamsplitter (Newport, Irvine, California) that follow allows for changing the polarization of the output beam such that s-polarization will go into the TIRF optical fiber and p-polarization will go to the FSD confocal fiber. To properly feed the large laser beam into the single-mode optical fiber, achromatic doublet lenses with a focal distance of 12.7 mm are placed on xy lens positioners in front of the optical fibers. Each fiber is mounted on xyz translational stages (Newport, Irvine, California) equipped with supplemental tilt mechanisms (pitch and yawl) to allow fine tuning of the laser-to-fiber alignment. Once the PCAOM Bragg angle is optimized, the other optical components are aligned. By automatically rotating the half-wave plate by 45 deg, one can change the output beam polarization, such that only one optical fiber receives the laser beam at one time. The beamsplitter is mounted on a rotating stage with a tilt

Table 2 Optical filters. The far right column of numbers relates to the part numbers in Fig. 2. All fluorescence filters were made by Chroma Technology (Brattleboro, Vermont).

Product code	Product name	Number
Microscope turret (TIRF and Epifluorescence filters)		1F
HQ560/20, HQ610/60, z568rdc	Custom 568-nm laser set	
HQ640/20, HQ700/75, z647rdc	Custom 647-nm laser set	
z488/20, HQ535/50, z488rdc	Custom 488-nm laser set	
HQ510, HQ700/75m, z514rdc	Custom 514-nm laser set	
U-M6061, IX2-MDICT	Analyzer cube for DIC	
Yokogawa beamsplitters		2F
HQ520LP	High throughput dichroic 488-nm laser line	
Z458/514 tpc	Dual pass beamsplitter 457-nm and 514-nm laser lines	
Z405/488/568/647 tpc	Quad pass beamsplitter 405-488-568-647-nm laser lines	
Emission filters (filter wheel)		3F
69687	HQ 440/40 m	
117985	ET 480/40 m	
118052	ET 525/50 m	
118071	ET 535/50 m	
115173	API ET 705/72 m	
63066	Z 458−514 m	
62935	Z 488−568 m	
69244	Z 405−488−568−647 m	
AFM Filters		
ET670sp	Eye piece and camera protection filter for AFM laser diode	4F
E680sp, lot 60144	Video camera filter	5F
D690/15x-HC	AFM head filter	6F

mechanism to allow easy alignment of the laser beam with the fibers. An initial laser-to-fiber alignment is performed using a multimode optical fiber provided by Oz Optics as an alignment tool. Once the power is maximized through the multimode fiber, this is replaced with the single-mode fibers that are connected at the output end with a custom-made mount into a Field Master powermeter (Coherent, Portland, Oregon). After locking in place the *xyz* mount, further fine alignment is performed using the tilt mechanism. Table 4 shows the laser power along different points in the optical train. All optical components are optimized for high laser power and have antireflective coatings.

4.2 Cameras and Software

The imaging system is equipped with QuantEM 512SC cameras (Roper Scientific Photometrics, Tuscon, Arizona). These are back-illuminated electron-multiplying (EM) CCD optimized for high speed and sensitivity over a wide dynamic range (16 bits). The EMCCD can be operated as: conventional CCD with no gain for high responsivity; EM with gain off for high signal strength; and EM with gain on for high sensitivity. A remote cooling fan is added to the Peltier cooling system. The EMCCD image sensor E2V CCD 97 has a 512×512 imaging array of 16×16-μm pixel size with a

Table 3 Component list of the integrated microscope. The far right column of numbers relates to the part numbers in Figure 2.

Company	Product code	Product name	Number
Dell	Precision 390	Precision workstation Windows XP Pro with dual 2-GHz XEON CPUs, 4-GB RAM, 667 MHz, 250-GB HD, nVidia Quadro FX3500 256-MB graphics card, dual monitors	
Intelligent Imaging		Roper Cascade QuantEM 512SC Peltier cooled with remote fan	1
Innovations	O31-YKGA	Yokagawa CSU-22 confocal head	2
		Slidebook 4.2.0.9 for Windows	
	O31-SYNC	TTL module	
		1.5× Optovar lens	
MDL Enterprise	PCM1000A-H4HB	Oneac 100VA medical grade power conditioner	
NEOS Technologies	12D4069, 12D2350	AOTF crystal 5-mm acoustic window and eight channel controller	3
New Focus	9064-XYZ, 9353	XYZ translation stage with micrometer 0 to 25 mm	
	900211	Big jack	4
Newport	RS4000-5′−8′−12″	Research-grade tabletop	
	I2000-423.5	Support system stabilizer vibration isolators	
	ACMP	Air compressor, 19 to 120 psi preset	
	ATS-8, ATS-CMC	Overhead table shelf and cable management system	
	PAC010AR.14	Achromatic doublet lens, 12.7-mm EFL, AR 430 to 700 nm	5
	LP-1A-XY	Two-axis lens positioner	6
	562F-XYZ, 562F-TILT, 561-FCA4	XYZ heavy duty stage, tilt module, and fiber connector	7
	SR50CC, SMC100CC	Rotary stage with controller	8
	UGP-1	Gimbaled prism mount	9
	10FC16PB.3	Beamsplitter polarizing cube	10
Olympus	IX81F2, UYCP-11	Motorized Olympus IX81, left/right adjustable port mounts; trinoc with Bertrand lens; illuminator pillar with 12-V / 100-W Halogen lamp (post tilts back 30 deg, rotating center section, attached condenser holder)	
	IX81-ZDC	Focus drift compensator	11
	5-UR478	IX2-RFAEVA2-TIRFM fiber illuminator class 3B	12
	1-U2B523	U Pl FLN 10× dry NA=0.3 Ph 1 WD=10 mm	
	1-U2C527	U PL FL 40× Ph2 dry NA=0.6 WD=0.51 mm	
	1-UB637F2	PLAN APO 60× W NA=1 WD=0.15 mm	
	1-U2B616	PLAN APON 60× TIRFM oil DIC NA 1.45 WD=0.1 mm	
	1-U2B836	UPLAN S APO 100× oil NA=1.46 DIC WD=0.12 mm	
	KP-M2AN	Hitachi B/W 1/2″ video camera	13
Optical Insights	Xtender	Collimated emission-port adapter	14

Table 3 (*Continued.*)

Company	Product code	Product name	Number
Oz Optics	QPMJ-A3HPM, FC/APC	High powered PM fiber patchcord 450 to 650 nm with FC air gap connector on one end and an angle FC/APC connector on the other end	15
	QPMJ-A3HPM FC/PC	High power PM patchcord 450 to 650 nm, with FC air gap connector on one end and straight FC/PC connector on the other end	16
Spectra Physics	2018-RM	Stabilite 2018 RM Ar/Kr (457 to 647 nm)	17
	315A-1S	Ion laser water conditioning system (25 KW capacity)	18
Sutter Instruments	LB 10-2	Ten positions filter wheel and Lambda 10-2 controller	19
ThorLabs	AHWP05M-630	Achromatic half-wave plate	20
Veeco	SPC-BIO1-TAM-JN	Hybrid head with custom slot filter	21
Instruments	NS4-01	Nanoscope IVa SPM controller	22
	SPC-BIO1-TAM-MT	Olympus IX2 baseplate and sample chuck for use with TIRF	23
		Workstation Windows NT 4.0 with 1.7 GHz Pentium 4 CPU, 256-MB RAM, 60-GB HD, video frame grabber (BIOFG)	

total imaging area of 8.2×8.2 mm, offering the highest available quantum efficiency at peak ($>90\ \%$). Two identical cameras are used, one on the confocal side, and one on the TIRF side.

The speed of image acquisition of this microscope is limited only by the camera speed acquisition. The main advantage of the EM technology is that it allows the detector to improve the signal-to-noise ratio of a low signal image. Thus, good detection of weak signals generated from dim samples or due to reduced time exposure because of high-speed detection is possible. The read noise contribution to the image is higher when the pixel read rate is higher. When running at high read rates, the increase in noise can be diminished by applying gain to the signal such that it will be amplified before it is read out. Thus, because the signal amplification takes place before the readout occurs, the signal is amplified while the read noise contribution remains the same for a given read rate.[46]

The quality of the FSD confocal image depends on how well the speed of the EMCCD camera is correlated with the speed of the tandem disk unit. The CSU 22 scanning head has a variable speed up to 5000 rot/min, which results in an acquisition speed as high as 1000 frames/sec if we take into consideration that the tandem-disk scans one image on a 12th from one full rotation. The FSD speed has to be correlated with the camera acquisition speed to avoid appearance of bands of light and dark in the image. Thus, the time necessary to scan one image at a given disk speed has to be correlated with the camera exposure time. This correlation can be achieved for any given camera exposure time of integer numbers of milliseconds for which the speed of the FSD can be controlled. We have been able to acquire images as fast as 50-ms exposure time with no binning and good image quality, which translates to 20 frames/sec. Faster acquisition speed is possible with lower resolution.

Due to the rectangular aperture of the spinning disk scanner [Fig. 2(a)], not all the field of view of the EMCCD camera will be illuminated. To take advantage of the full field of view, a $1.5\times$ lens is placed in front of the camera that allows a true magnification of the projected image on the camera chip.

The AFM requires a video camera (Hitachi 2/3-in. B/W) that is mounted on a trinocular port. This is used for precise positioning of the AFM tip on the cell surface.

Instrument calibration presents important challenges in obtaining a good spatial and temporal match between the AFM and optical imaging methods. The field of view of the AFM

Table 4 Laser power measurements. All values were measured at 36 A. Actual imaging experiments were performed with 20-mW end-of-fiber output for all lines.

Total power 1.5 W	488 nm	514 nm	568 nm	647 nm
Dispersive prism (beam optimized for power)	380 mW	300 mW	180 mW	300 mW
White mode-w/AOTF (beam optimized for mode not for power)	340 mW	60 mW	82 mW	76 mW
End of fiber-S-polarization	50 mW	22 mW	62 mW	23 mW
End of fiber-p-polarization	43 mW	25 mW	47 mW	20 mW

and optical imaging need an excellent match in the x-y axes to limit off-line image correlation.

The first step of alignment consists in positioning the very end of the AFM tip on the microscope optical axis. This step consist of visualizing the AFM tip on a video camera (that is inherently aligned with the microscope optical path) and sliding the baseplate of the AFM stage such that the very end of the AFM tip is centered in the image (due to design constraints of the AFM scanner, the AFM tip is actually decentered from the vertical axis of the scanner).

The second step of alignment consists in aligning the optical path of the FSD confocal with the microscope output on the left port. This is done by initially coupling the confocal unit to the microscope by the threaded flange, such that the height of the microscope is adjusted in small steps to match the position of the flange. Next, the filter wheel and finally the EMCCD camera are adjusted by xyz positioning. Once all of these elements are fixed in place, small adjustments of the microscope height will be made with the flange open, such that no movements in the camera field of view will be recorded. The EMCCD camera on the confocal side will function as the primary camera of the system. Due to differences in the field of view of the video camera compared with the EMCCD camera, it is important that a good optical alignment is performed, otherwise the AFM tip may be out of the field of view of the EMCCD.

The third step consists of aligning the TIRF camera in hardware, pixel for pixel, with the primary camera. For easy alignment of these cameras, special brackets were designed and the cameras were placed on xyz stages. A grid is used to align these two cameras. Thus, by capturing sequential images of the grid on both cameras, small position adjustments on the TIRF camera are done until the images overlap in software.

SlideBook software (Intelligent Imaging Innovations, Denver, Colorado) is used to control the acquisition and data processing of the optical imaging, and Nanoscope 6.14R1 software (Veeco Instruments, Santa Barbara, California) is used to control the AFM. The software offers a user-friendly interface, where the optical configurations of the microscope can be user-defined such that different filters and other optical components, including scanning-head settings, laser power, and laser line, can be programmed.

5 Single-Cell Applications

5.1 Cell Culture and Transfections

The isolation of VSMC has been previously described.[47] Cells were cultured on glass bottom cell culture dishes (MatTek, Ashland, Massachusetts) in 5% CO_2 at 37°C in supplemented Dulbecco's Modified Eagle Medium (Invitrogen, Carlsbad, CA). Transient transfections were performed using Amaxa Nucleofector apparatus (Gaithersburg, Maryland) with nucleofector kit VPI1004 per the manufacturer's protocol (program E-033): 500 k cells per reaction were nucleofected with the indicated fluorescent plasmids (1 to 2 μg each) and were seeded at 60 k cells per 60-mm dish. A high transfection efficiency was recorded (>70 %). Imaging experiments were performed 24 h after transfections.

Epithelial liver cells Clone 9 (ATCC, CRL 1439) were used between passage 25 to passage 30. Cells were cultured as above and loaded with 3-μM Fluo-4 AM (Invitrogen,

Carlsbad, CA) for one hour at 37°C, and then washed and imaged in serum- and phenol red- free medium. Cells were treated with vasopressin (V-0377, Sigma, St. Louis, MO) at 2 nM to induce calcium oscillations as previously characterized in Ref. 48.

5.2 Live Cell Imaging

In this section, several applications of the integrated AFM-optical imaging microscope are presented.

In Fig. 4 vascular smooth muscle cells (VSMC) were imaged in AFM mode to show cell topography. TIRF and confocal images of the same cell, transfected as above, were acquired immediately following acquisition of the AFM image. An excellent registration between the AFM image and the TIRF and FSD confocal fluorescence images can be achieved as shown in the overlays [Figs 4(d) and 4(e)]. AFM provides a general topographic view of the cell with few actin cytoskeletal fibers immediately beneath the membrane. The confocal image reveals a multitude of actin fibers aligned along the cell axis. If TIRF images are compared with FSD confocal images of the same cell, more background from the cell body is shown by the confocal images. Not all actin fibers are present in the AFM image, because the AFM tip senses only features immediately beneath the cell membrane. The fluorescence from the actin fibers (actin-mRFP) inside the cell body, as well as focal adhesions (vinculin-GFP) are obvious in the confocal and TIRF images. TIRF images were acquired sequentially with an exposure time of 100 ms, and FSD confocal images were acquired as a two-channel 3-D stack of 20 planes with the same exposure time and presented as maximum projection.

Figure 5 shows confocal images of VSMC subjected to mechanical stimulation applied by AFM to the apical cell surface. The mechanical stimulation was induced by a functionalized AFM probe (2-μm glass bead coated with fibronectin), which was set at a chosen xy coordinate on the cell surface and moved upward in discrete steps as described in Ref. 1. Following each controlled upward movement of the functionalized cantilever tip along the z axis (the position of which is shown by white dashed lines), the cell responds to the mechanical stimulation. Confocal images of the same VSMC, transfected with actin-mRFP, before and after AFM stimulation, show that the cell significantly modified its shape, such that actin filaments reorganized in almost a regular pattern of parallel actin bundles following the long axis of the cell. Moreover, the xz and yz side view images of the same cell (see arrows) obtained by 3-D image reconstruction from consecutive confocal sectioning of the cell show an increase in cell height after the mechanical stimulation, as well as a redistribution of the actin filaments toward the bottom of the cell.

Video 1 shows real-time cell shrinkage and FA rearrangement due to AFM mechanical stimulation. TIRF images of VSMC transfected with actin-mRFP and vinculin-GFP show that F-actin is recruited at the bottom of the cell in the immediate vicinity of the FA that also reorganizes to better anchor the cell to the substrate to oppose the applied force. The TIRF images were acquired during the AFM stimulation experiment with 100-ms exposure time at eight time points between 0 and 80 min. The video is shown at 1.5 frames/sec.
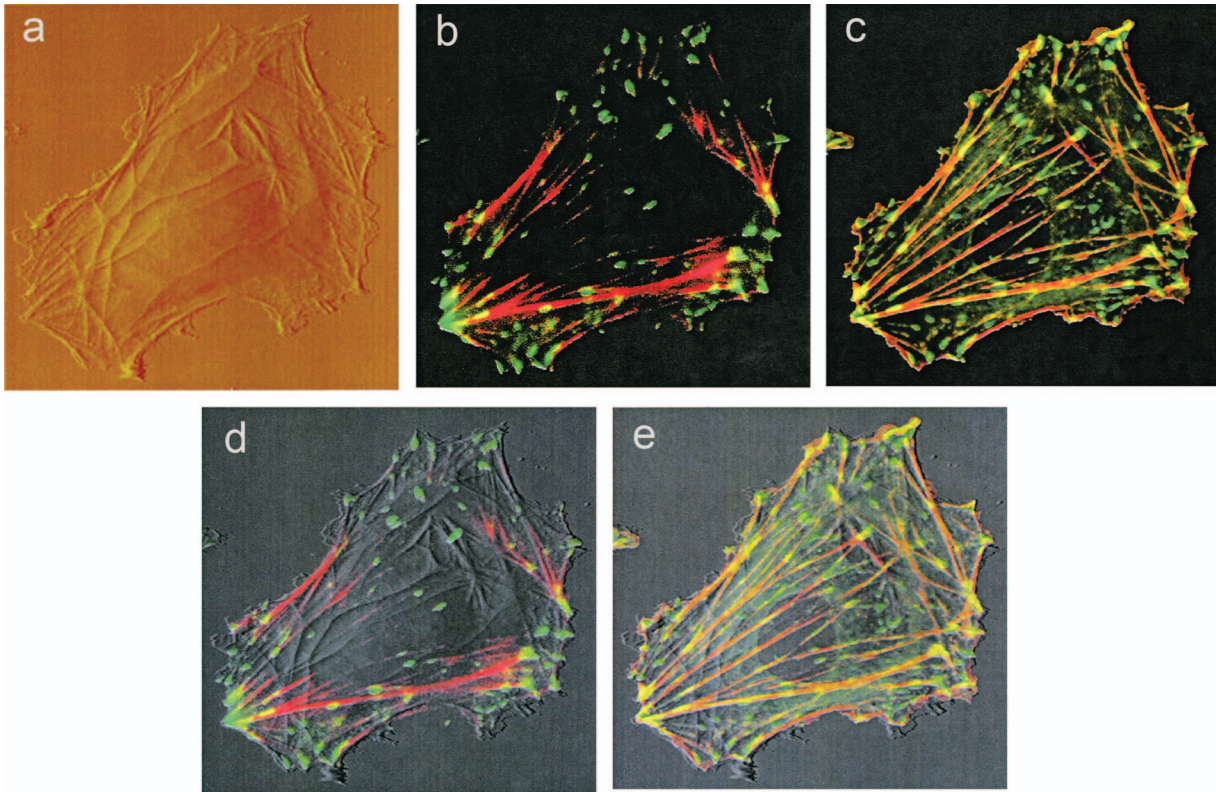
Fig. 4 Same VSMC transfected with mRFP-actin and vinculin-GFP was imaged by: (a) AFM at the apical cell surface; (b) TIRF at the basal cell surface; and (c) FSD confocal throughout the cell body is shown as maximum projection of a 3-D stack. Excellent overlaps between the AFM and TIRF or FSD confocal images are shown in (d) and (e), respectively. The stress fibers present in the AFM image overlay with actin fibers from the fluorescence images. Image size is 66×64 μm.
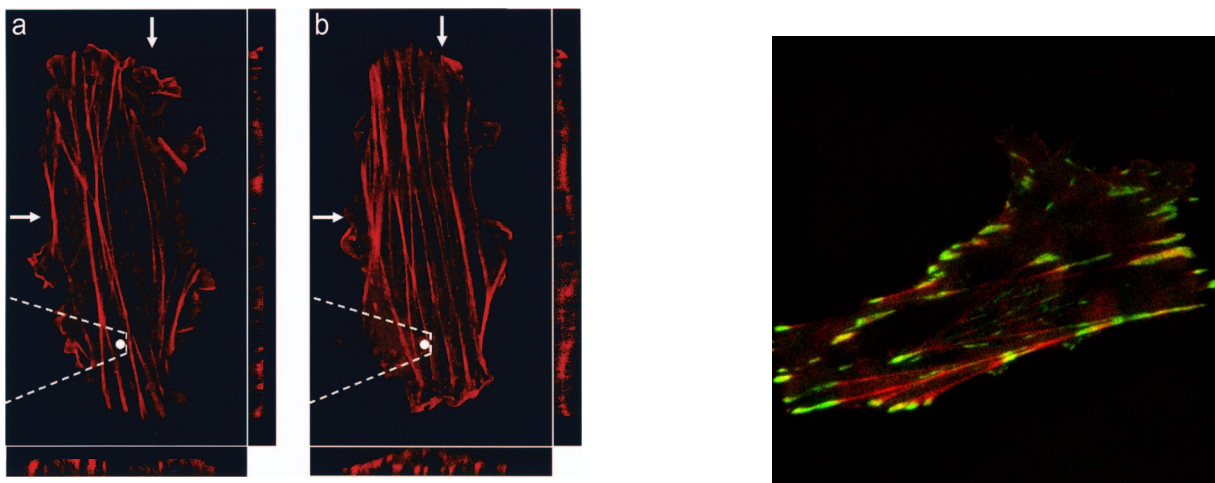

Fig. 5 VSMC transfected with mRFP-actin were imaged by FSD confocal before (a) and after (b) AFM mechanical stimulation. Following mechanical stimulation, actin filaments reorganized in almost a regular pattern of parallel bundles along the cell axis. The side views show actin reorganization and recruitment toward the cell bottom along the indicated section in the xz and yz planes (see arrows). White dashed lines represent the AFM tip above the cell. Image size is 50×86 μm.

Video 1. Real-time cell restructuring shown as time-lapse images acquired in TIRF mode for the duration of the experiment (~ 80 min). VSMC were transfected with vinculin-GFP and actin-mRFP. The images were acquired with 100-ms exposure time at eight time points between time 0 and 80 min. The video is shown at 1.5 frames/sec. Image size is 91×91 μm. (QuickTime, 2.36 Mb). [URL: http://dx.doi.org/10.1117/1.3155517.1]
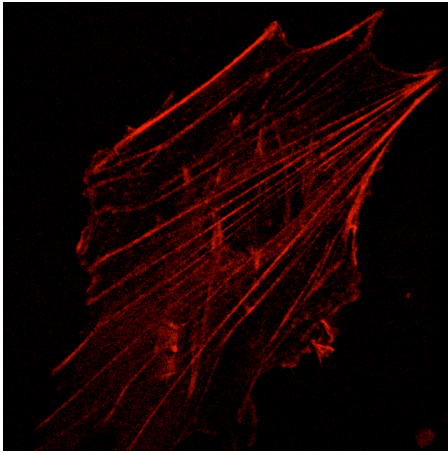
Video 2. Real-time actin fibers restructuring shown as 3-D time-lapse video from FSD confocal imaging of VSMC transfected with actin-mRFP. The images were acquired with 100-ms exposure time as a 3-D stack of 20 planes at six time points between time 0 and 80 min. The video is shown at 1 frame/sec. A small reflection of the fluorescence due to the AFM tip is also visible. (QuickTime, 1.75 Mb).
[URL: http://dx.doi.org/10.1117/1.3155517.2]

Video 2 shows real-time actin restructuring due to AFM mechanical stimulation. Time-lapse 3-D stacks were acquired using FSD confocal for the duration of the experiment (∼80 min). The arrows in Fig. 6 (the first frame of the video) indicate actin fibers that disappear (a), thin out due to actin restructuring (b), and bend due to the mechanical stimulation (c). The AFM tip above the cell is shown by white dashed lines. Images were acquired with 100-ms exposure time as a 3-D stack of 20 planes at six time points between time 0 and 80 min. The video is shown at 1 frame/sec.
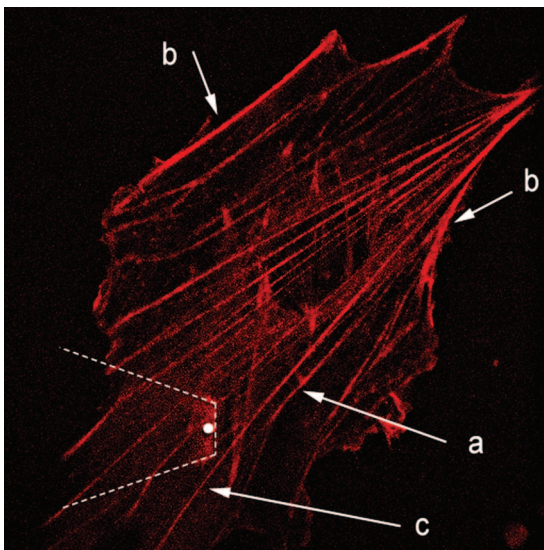
Fig. 6 A VSMC transfected with mRFP-actin was imaged by FSD confocal. The arrows indicate actin fibers that show remarkable restructuring: (a) actin fibers disappear, (b) actin fibers thin out due to actin restructuring, and (c) actin fiber bends due to the mechanical stimulation (see text). The AFM tip above the cell is shown by white dashed lines. Image size is 91×91 μm (see Video 2)
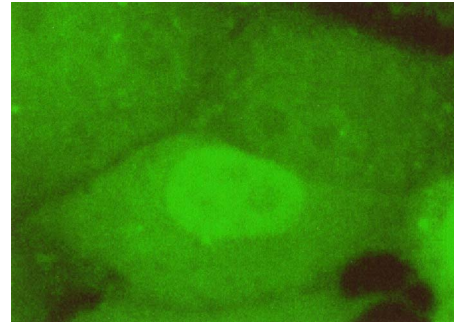
Video 3. Time-lapse movie of FSD confocal images of calcium oscillations in liver epithelial cells, induced by vasopressin treatment, acquired with 60-ms exposure time. The video is shown at 5 frames/sec. Image size is 40×28 μm. (QuickTime, 1.66 Mb).
[URL: http://dx.doi.org/10.1117/1.3155517.3]

The basal cell area was reduced $8.7 \pm 2.1\%$ after AFM mechanical stimulation, but the vinculin area increased $11.1 \pm 2.1\%$ (n=5). Also, F-actin at the basal cell area (TIRF images) increased $16.9 \pm 1.9\%$ and F-actin in whole cell volume (confocal images) increased $8.2 \pm 0.3\%$ (n=4). By recruiting FA proteins and F-actin at the basal cell area, the cell reinforces its attachment to the substrate to better resist the mechanical stimulation. Area measurements were performed in SlideBook software (Intelligent Imaging Innovations, Denver, Colorado). The percent change in protein area was calculated as percent change=[(treatment-control)/control] $\times 100$. Therefore, a significant rearrangement of the actin filaments and FA took place due to the local mechanical cell stimulation at the apical cell membrane that induced changes into the cellular structure throughout the cell body.

Examples of the utility of the integrated microscope to examine the restructuring of actin filaments and FA as the result of mechanical stimulation to the surface of cells have been presented. Another application under development is the analysis of FA reorganization as a function of forces generated from within cells. Videos 3 and 4 show calcium oscillations in liver epithelial cells Clone 9 (ATCC, Manassas, VA), the fre-
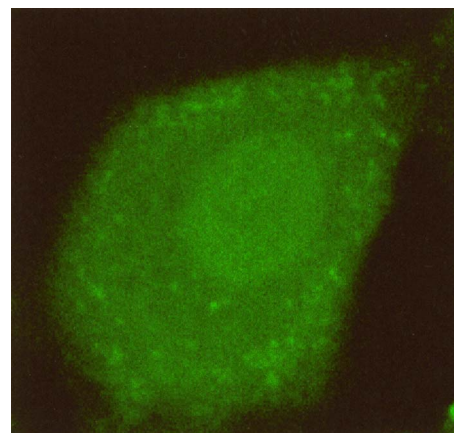
Video 4. Time-lapse video of FSD confocal images of calcium oscillations in a single liver epithelial cell, induced by vasopressin treatment, acquired with 50-ms exposure time at 20 frames/sec. Image size is 37×35 μm. (QuickTime, 8.88 Mb).
[URL: http://dx.doi.org/10.1117/1.3155517.4]

quency of which is dependent on agonist concentration as previously characterized.[48] By treating the cells with 2-nM vasopressin, intracellular calcium oscillations are induced at about 50 mHz. Video 3 was acquired as time-lapse 3-D stack for each time point at 3 frames/sec in FSD confocal microscopy. For Video 4, we were able to acquire images as fast as 50-ms exposure time with no binning and good image quality, which translates to 20 frames/sec and shows details of two calcium oscillations in the same cell. These frequency-encoded calcium signals activate key signaling pathways that mediate myosin-light-chain-dependent contractions, which are transmitted by FA to the extracellular matrix, and can be studied by AFM-optical imaging combined experiments.

6 Concluding Remarks

Cells have dynamic structures that adapt continuously to their micromechanical environment. The importance of the external mechanical stimuli that determine profound changes intracellularly can be seen in pathological conditions as hypertension, atherosclerosis, or inflammation. Fundamental understanding of the mechanotransduction process, and of the cellular pathological responses, will allow new insights into understanding the structure-function relationships of cells. The most interesting cellular behaviors are highly dynamic and occur locally in specific cell regions: cell signaling response to mechanical stimulation, FA and actin turnover, protein translocation, conformational changes of proteins, etc. Thus, particular cellular phenomena have their own time and distance scales that have to be matched by the instruments that we use to analyze them.

The technology presented here is broadly applicable across a wide range of molecular dynamic studies in any adherent live cells. By integrating in one instrument the AFM with TIRF and FSD confocal microscopy, we are able to follow and quantify specific adhesion proteins or cytoskeletal rearrangement and cell signaling in real time. This instrument enables future studies of 3-D spatial optical imaging of molecular dynamics in different subcellular structures at a time scale of milliseconds while applying mechanical stimulation forces in the range of pico- to nano-Newtons. Cell response to various types of agonist or mechanical stimulation can be observed directly, and the dynamics and characteristics of reorganization at subcellular level may be studied in real time.

References

1. A. Trache and G. A. Meininger, "Atomic force—multi optical imaging integrated microscope for monitoring molecular dynamics in live cells," *J. Biomed. Opt.* **10**(6), 064023 (2005).
2. G. Binnig, C. F. Quate, and C. H. Gerber, "Atomic force microscope," *Phys. Rev. Lett.* **56**(9), 930–933 (1986).
3. S. Inoue and T. Inoue, "Direct-view high-speed confocal scanner: the CSU-10," *Methods Cell Biol.* **70**, 87–127 (2002).
4. D. Axelrod, "Selective imaging of surface fluorescence with very high aperture microscope objectives," *J. Biomed. Opt.* **6**(6), 6–13 (2001).
5. D. E. Ingber, L. Dike, L. Hansen, S. Karp, H. Liley, A. Maniotis, H. McNamee, D. Mooney, G. Plopper, J. Sims, and N. Wang, "Cellular tensegrity: exploring how mechanical changes in the cytoskeleton regulate cell growth, migration, and tissue pattern during morphogenesis," *Int. Rev. Cytol.* **150**, 173–224 (1994).
6. Y. Sawada and M. P. Sheetz, "Force transduction by Triton cytoskeletons," *J. Cell Biol.* **156**(4), 609–615 (2002).
7. J. R. Sims, S. Karp, and D. E. Ingber, "Altering the cellular mechanical force balance results in integrated changes in cell, cytoskeletal and nuclear shape," *J. Cell. Sci.* **103**(4), 1215–1222 (1992).
8. N. F. Worth, B. E. Rolfe, J. Song, and G. R. Campbell, "Vascular smooth muscle cell phenotypic modulation in culture is associated with reorganization of contractile and cytoskeletal proteins," *Cell Motil. Cytoskeleton* **49**(3), 130–145 (2001).
9. J. D. Humphries, P. Wang, C. Streuli, B. Geiger, M. J. Humphries, and C. Ballestrem, "Vinculin controls focal adhesion formation by direct interactions with talin and actin," *J. Cell Biol.* **179**(5), 1043–1057 (2007).
10. Y. L. Hu, J. H. Haga, H. Miao, Y. Wang, Y. S. Li, and S. Chien, "Roles of microfilaments and microtubules in paxillin dynamics," *Biochem. Biophys. Res. Commun.* **348**(4), 1463–1471 (2006).
11. J. Pourati, A. Maniotis, D. Spiegel, J. L. Schaffer, J. P. Butler, J. J. Fredberg, D. E. Ingber, D. Stamenovic, and N. Wang, "Is cytoskeletal tension a major determinant of cell deformability in adherent endothelial cells?" *Am. J. Physiol.: Cell Physiol.* **274**(5), C1283–C1289 (1998).
12. P. A. Janmey, "The cytoskeleton and cell signaling: component localization and mechanical coupling," *Physiol. Rev.* **78**(3), 763–775 (1998).
13. A. O. Saez, W. Zhang, Y. Wu, C. E. Turner, D. D. Tang, and S. J. Gunst, "Tension development during contractile stimulation of smooth muscle requires recruitment of paxilin and vinculin to the membrane," *Am. J. Physiol.: Cell Physiol.* **286**(2), C433–C447 (2004).
14. F. J. Alenghat and D. E. Ingber, "Mechanotransduction: all signals point to cytoskeleton, matrix and integrins," *Sci. STKE* **2002**(119), 1–4 (2002).
15. E. Zamir and B. Geiger, "Molecular complexity and dynamics of cell-matrix adhesions," *J. Cell. Sci.* **114**(20), 3583–3590 (2001).
16. T. P. Lele, C. K. Thodeti, and D. E. Ingber, "Force meets chemistry: analysis of mechanochemical conversion in focal adhesions using fluorescence recovery after photobleaching," *J. Cell. Biochem.* **97**(6), 1175–1183 (2006).
17. B. Geiger and A. Bershdsky, "Assembly and mechanosensory function of focal contacts," *Curr. Opin. Cell Biol.* **13**(5), 584–592 (2001).
18. H. R. Romer, K. G. Birukov, and J. G. N. Garcia, "Focal adhesions.

Paradigm for a signaling nexus," *Circ. Res.* **98**(5), 606–616 (2006).

19. S. K. Sastry and K. Burridge, "Focal adhesions: a nexus for intracellular signaling and cytoskeletal dynamics," *Exp. Cell Res.* **261**(1), 25–36 (2000).

20. K. Burridge and M. Chrzanowska-Wodnicka, "Focal adhesions, contractility and signaling," *Annu. Rev. Cell Dev. Biol.* **12**, 463–518 (1996).

21. R. Zaidel-Bar, R. Milo, Z. Kam, and B. Geiger, "A paxillin tyrosine phosphorylation switch regulates the assembly and form of cell-matrix adhesions," *J. Cell. Sci.* **120**(Pt 1), 137–48 (2007).

22. D. Tang, D. Mehta, and S. J. Gunst, "Mechanosensitive tyrosine phosphorylation of paxillin and focal adhesion kinase in tracheal smooth muscle," *Am. J. Physiol.: Cell Physiol.* **276**(1), C250–258 (1999).

23. C. E. Turner, "Paxillin and focal adhesion signaling," *Nat. Cell Biol.* **2**(12), E231–E236 (2000).

24. M. Yoshigi, L. M. Hoffman, C. C. Jensen, H. J. Yost, and M. C. Beckerle, "Mechanical force mobilizes zyxin from focal adhesions to actin filaments and regulates cytoskeletal reinforcement," *J. Cell Biol.* **171**(2), 209–215 (2005).

25. M. Cattaruza, C. Lattrich, and M. Hecker, "Focal adhesion protein Zyxin is a mechanosensitive modulator of gene expression in vascular smooth muscle cells," *Hypertension* **43**(4), 726–730 (2004).

26. Y. Wang and T. D. Gilmore, "Zyxin and paxillin proteins: focal adhesion plaque LIM domain proteins go nuclear," *Biochim. Biophys. Acta* **1593**(2–3), 115–120 (2003).

27. R. Y. Tsien, "Imagining imaging's future," *Nat. Rev. Mol. Cell Biol.* **4**, Suppl. SS16–21 (2003).

28. D. Axelrod and G. M. Omann, "Combinatorial microscopy," *Nat. Rev. Mol. Cell Biol.* **7**(12), 944–952 (2006).

29. S. R. Heidemann and D. Wirtz, "Towards a regional approach to cell mechanics," *Trends Cell Biol.* **14**(4), 160–166 (2004).

30. K. J. Van Vliet, G. Bao, and S. Suresh, "The biomechanics toolbox: experimental approaches for living cells and biomolecules," *Acta Mater.* **51**(19), 5881–5905 (2003).

31. M. C. Adams, W. C. Salmon, S. L. Gupton, C. S. Cohan, T. Wittmann, N. Prigozhina, and C. M. Waterman-Storer, "A high-speed multispectral spinning-disk confocal microscope system for fluorescent speckle microscopy of living cells," *Methods* **29**(1), 29–41 (2003).

32. R. J. Graf, J. Rietdorf, and T. Zimmermann, "Live cell spinning disk microscopy," *Adv. Biochem. Eng./Biotechnol.* **95**, 57–75 (2005).

33. E. Wang, C. M. Babbey, and K. W. Dunn, "Performance comparison between the high-speed Yokogawa spinning disc confocal system and single-point scanning confocal systems," *J. Microsc.* **218**(Pt 2), 148–159 (2005).

34. D. Axelrod, N. L. Thompson, and T. P. Burghardt, "Total internal reflection fluorescent microscopy," *J. Microsc.* **129**, 19–28 (1983).

35. D. Axelrod, T. P. Burghardt, and N. L. Thompson, "Total internal reflection fluorescence," *Annu. Rev. Biophys. Bioeng.* **13**, 247–268 (1984).

36. A. Stout and D. Axelrod, "Evanescent field excitation of fluorescence by epi-illumination microscopy," *Appl. Opt.* **28**(24), 5237–5242 (1989).

37. W. M. Reichert, "Evanscent detection of absorbed films: assessment of optical considerations for absorbance and fluorescence spectroscopy at the crystal/solution and polymer/solution interfaces," *Crit. Rev. Biocompat.* **5**, 173–205 (1989).

38. W. M. Reichert and G. A. Truskey, "Total internal reflection fluorescence (TIRF) microscopy. I. Modeling cell contact region fluorescence," *J. Cell. Sci.* **96**(2), 219–230 (1990).

39. J. S. Burmeister, L. A. Olivier, G. A. Truskey, and W. M. Reichert, "Application of total internal reflection fluorescence microscopy to study cell adhesion to biomaterials," *Biomaterials* **19**(4–5), 307–325 (1998).

40. M. Radmacher, R. W. Tillman, M. Fritz, and H. E. Gaub, "From molecules to cells: imaging soft samples with the atomic force microscope," *Science* **257**(5078), 1900–1905 (1992).

41. M. Gad and A. Ikai, "Imaging living cells and mapping their surface molecules with the atomic force microscope," in *Methods in Cellular Imaging*, A. Periasamy, Ed., pp. 409–423 (2001).

42. A. Trache, J. P. Trzeciakowski, L. Gardiner, Z. Sun, M. Muthuchamy, M. Guo, S. Y. Yuan, and G. A. Meininger, "Histamine effects on endothelial cell fibronectin interaction studied by atomic force microscopy," *Biophys. J.* **89**(4), 2888–2898 (2005).

43. H. J. Butt, B. Cappella, and M. Kappl, "Force measurements with atomic force microscope: technique, interpretation and applications," *Surf. Sci. Rep.* **59**(1–6), 1–152 (2005).

44. O. H. Willemsen, M. M. Snel, A. Cambi, J. Greve, B. G. De Grooth, and C. G. Figdor, "Biomolecular interactions measured by atomic force microscopy," *Biophys. J.* **79**(6), 3267–3281 (2000).

45. E. P. Wojcikiewicz, X. Zhang, and V. T. Moy, "Force and compliance measurements on living cells using atomic force microscopy (AFM)," *Bio. Proceed Online* **6**, 1–9 (2004).

46. F. Chong, C. G. Coates, D. J. Denvir, N. McHale, K. Thornbury, and M. Hollywood, "Optimization of spinning disk confocal microscopy: synchronization with the ultra-sensitive EMCCD," *Proc. SPIE* **5324**, 65–76 (2004).

47. X. Wu, G. E. Davis, G. A. Meininger, E. Wilson, and M. J. Davis, "Regulation of the L-type calcium channel by alpha 5-beta 1 integrin requires signaling between focal adhesion proteins," *J. Biol. Chem.* **276**(32), 30285–30292 (2001).

48. R. Barhoumi, Y. Mouneimne, I. Awooda, S. H. Safe, K. C. Donnelly, and R. C. Burghardt, "Characterization of calcium oscillations in normal and benzo[a]pyrene-treated Clone 9 cells," *Toxicol. Sci.* **68**(2), 444–450 (2002).